

ARTICLES

 $b\bar{b}$ spectroscopy from the $\Upsilon(3S)$ state

U. Heintz,* J. Lee-Franzini, D. M. J. Lovelock,† M. Narain,‡ R. D. Schamberger, J. Willins,
and C. Yanagisawa

State University of New York at Stony Brook, Stony Brook, New York 11794

P. Franzini, S. Kanekal, P. M. Tuts, and Q. W. Wu

Columbia University, New York, New York 10027

(Received 30 September 1991)

Using the CUSB-II detector at CESR we have observed electric dipole transitions between the Υ and χ_b states, both in exclusive and inclusive channels. We have measured their branching ratios and find $B(\Upsilon(3S) \rightarrow \chi_b(2P_{2,1,0})\gamma) = (11.1 \pm 0.5 \pm 0.4)\%$, $(11.5 \pm 0.5 \pm 0.5)\%$, $(6.0 \pm 0.4 \pm 0.6)\%$. We have measured the center of gravity of the $\chi_b(2P)$ states to be $(10259.5 \pm 0.4 \pm 1.0)$ MeV and their fine-structure mass splittings to be $(13.5 \pm 0.4 \pm 0.5)$ MeV between the $J=2$ and $J=1$ states and $(23.5 \pm 0.7 \pm 0.7)$ MeV between $J=1$ and $J=0$, leading to a fine-structure ratio of $0.574 \pm 0.024 \pm 0.02$. The measured fine-structure splitting implies that the spin-orbit interaction dominates over the tensor interaction and that the long-range confining potential is due to an effective scalar exchange. From the measured branching ratios we infer the hadronic widths of the $\chi_b(2P)$ states and find them to be consistent with QCD predictions. We use them to derive values of α_s . We have observed the suppressed transition $\Upsilon(3S) \rightarrow \chi_b(1P)\gamma$ and the $\pi^0\pi^0$ transitions from the $\Upsilon(3S)$. We find $B(\Upsilon(3S) \rightarrow \Upsilon(1S)\pi^0\pi^0) = (2.2 \pm 0.4 \pm 0.3)\%$ and $B(\Upsilon(3S) \rightarrow \Upsilon(2S)\pi^0\pi^0) = (1.7 \pm 0.5 \pm 0.2)\%$. We also present a measurement of the dipion invariant-mass spectrum from the transition $\Upsilon(3S) \rightarrow \Upsilon(1S)\pi^0\pi^0$.

PACS number(s): 14.40.Gx, 13.25.+m, 13.40.Hq

I. INTRODUCTION

During the past two decades, the study of heavy quarkonia has contributed to the confirmation of the quark model and given us new insight into the interactions of quarks and gluons. Heavy quarkonia are bound states of a heavy quark and its antiquark. They provide us with a simple nonrelativistic system to study the strong interaction. Because of its high mass and rich level spectrum the $b\bar{b}$ system is particularly suitable for these studies. A good phenomenological description of the properties of heavy quarkonia, their masses and transition rates, has been obtained from potential models.

Electron-positron colliders provide a particularly clean way of studying the $b\bar{b}$ system. Triplet S states, which are called Υ and have the same quantum numbers as the photon, are produced via single-photon annihilation of an e^+e^- pair. Therefore only the decay products of the Υ are left in the final state. States with other quantum numbers can be observed in the decay of triplet S states.

Below the open flavor threshold $b\bar{b}$ states can decay either by annihilation of their b quarks or via electromagnetic or hadronic transitions to lighter $b\bar{b}$ states. There

are three triplet S states below threshold, the ground state $\Upsilon(1S)$, and two excited states $\Upsilon(2S)$ and $\Upsilon(3S)$. They annihilate predominantly through a three-gluon (ggg) intermediate state to hadrons. However, annihilation via a photon and two gluons (γgg) or into lepton (l^+l^-) or quark ($q\bar{q}$) pairs via a single photon is also allowed. Two triplet P states, called $\chi_b(1P)$ and $\chi_b(2P)$, have been observed below threshold. They split into fine-structure levels with spins 2, 1, and 0. The states with even spin annihilate into two gluons (gg), while the state with spin one annihilates dominantly into a quark pair and a gluon ($q\bar{q}g$).

By running at the $\Upsilon(3S)$ energy a large number of transitions within the $b\bar{b}$ system become accessible. From 1983 to 1990 the CUSB-II detector at the Cornell Electron Storage Ring (CESR) has accumulated 288 pb^{-1} of data at the $\Upsilon(3S)$ resonance. We have used this data sample to perform detailed measurements of the $b\bar{b}$ system. By measuring the fine structure of the $\chi_b(2P)$ states we obtain information about the Lorentz character of the confining force. Their hadronic widths provide a test of QCD predictions of quark annihilation rates. There are two complementary methods to study these states. The "inclusive" method [1] consists of a study of the inclusive photon spectrum from hadronic $\Upsilon(3S)$ decays. The transition $\Upsilon(3S) \rightarrow \chi_b(2P)\gamma$ gives rise to narrow lines in this spectrum. This method takes advantage of the large hadronic branching fraction of the $b\bar{b}$ states. However, the signal has to be extracted from a large photon background, mainly due to π^0 decays. In the "exclusive"

*Present address: Columbia University, Nevis Laboratories, P.O. Box 137, Irvington, NY 10533.

†Present address: Medical Physics, Memorial Sloan-Kettering Cancer Center, 1275 York Avenue, New York, NY 10021.

‡Present address: Fermilab, P.O. Box 500, MS 357, Batavia, IL 60510.

method [2] we search for electromagnetic cascade events from the process $\Upsilon(3S) \rightarrow \chi_b(2P)\gamma \rightarrow \Upsilon\gamma\gamma$. We identify the Υ in the final state, which can be an $\Upsilon(1S)$ or an $\Upsilon(2S)$, by its decay to a $\mu^+\mu^-$ or e^+e^- pair. Because of the low multiplicity of these events they can be identified with very little background. However, the available number of events is small, due to the small leptonic branching ratio of the Υ states.

We have also used the exclusive method to investigate a number of other decay channels. We have observed events due to the suppressed cascade $\Upsilon(3S) \rightarrow \chi_b(1P)\gamma \rightarrow \Upsilon(1S)\gamma\gamma$, set an upper limit on $\Upsilon(1D)$ production in the double cascade $\Upsilon(3S) \rightarrow \chi_b(2P)\gamma \rightarrow \Upsilon(1D)\gamma\gamma$, $\Upsilon(1D) \rightarrow \chi_b(1P)\gamma \rightarrow \Upsilon(1S)\gamma\gamma$, and measured the $\pi^0\pi^0$ transitions $\Upsilon(3S) \rightarrow \Upsilon\pi^0\pi^0$.

The following two sections briefly describe the CUSB-II detector, trigger and event classification. Section IV describes the analysis of the inclusive photon spectrum, Sec. V the analysis of the exclusive events. The results of the analysis are interpreted in Secs. VI and VII. Section VI deals with the fine structure of the $\chi_b(2P)$ states, Sec. VII with their hadronic widths. Section VIII describes the measurement of the $\pi^0\pi^0$ transitions.

II. THE CUSB-II DETECTOR

It is our goal to resolve the fine structure of the $\chi_b(2P)$ states in the signal from the transition $\Upsilon(3S) \rightarrow \chi_b(2P)\gamma$. Good photon energy resolution is therefore the most important property of the detector. The CUSB-II detector was specifically designed for $b\bar{b}$ spectroscopy. It is a non-magnetic, highly segmented electromagnetic calorimeter, consisting of a cylindrical array of 360 bismuth germanate (BGO) crystals, 12 radiation lengths deep, which surrounds the beam pipe and covers about $\frac{2}{3}$ of the solid angle. The BGO crystals are arranged in 36 azimuthal sectors, five radial layers, and two polar halves. They are backed up by a similarly segmented array of NaI crystals, 8 radiation lengths deep, and 7 radiation lengths of lead glass. A charged particle veto is provided by a small drift chamber located inside the BGO cylinder. Scintillation counters surround the calorimeter to detect collinear muon pairs from Υ decays and a scintillator end cap increases the solid angle coverage of the detector for nearly collinear pairs of energetic leptons. The calorimeter crystals are calibrated using radioactive sources which have been embedded between the crystals. Source peaks are acquired through a special high-gain data path in the time between beam crossings. A detailed description of the detector can be found elsewhere [3].

III. TRIGGER AND EVENT CLASSIFICATION

We employ four hardware triggers. The most important trigger is a total energy trigger. It requires at least 800 MeV in the BGO array. This trigger is fully efficient for hadronic Υ decays within the solid angle coverage of our detector. Exclusive events with a decay of the final Υ state to a muon pair do not always deposit enough energy in the detector to fire the total energy trigger. For these events we need more sophisticated triggers. These are the two-muon trigger, which requires two hits in diagonally

opposite scintillation counters in coincidence with the beam crossing and energy depositions of 100 MeV each in the BGO and NaI arrays, and the distributed energy trigger, which requires 85 MeV in two diagonally opposite NaI octants and 275 MeV in BGO. The end-cap trigger requires hits in diagonally opposite end-cap scintillators in coincidence with the beam crossing and 210 MeV in the BGO. It extends the solid angle coverage of the detector for nearly collinear lepton pairs from exclusive events, beyond the central calorimeter. The distributed energy and end-cap triggers have only been available for the second half of the data taking period.

We use the longitudinal segmentation of the calorimeter to distinguish between minimum ionizing tracks, caused by fast muons or charged hadrons, and electromagnetic showers, caused by photons, electrons, and positrons. To identify minimum ionizing tracks we calculate a track quality Q for every sector in the calorimeter. Q is defined as

$$Q = \frac{1}{10} \frac{A}{|A - G|}, \quad (3.1)$$

where A is the arithmetic and G the geometric mean of energy depositions per unit path length (dE/dx) in the five layers of BGO or NaI. For a uniform dE/dx pattern A and G are approximately equal. Therefore for minimum ionizing particles Q is large while it is small for electromagnetic showers that show a longitudinal variation in their energy depositions.

Tracks in the drift chamber which point towards showers in the calorimeter identify charged particles.

IV. INCLUSIVE PHOTON SPECTRUM

To obtain the inclusive photon energy spectrum from hadronic $\Upsilon(3S)$ decays we use a sample of 1.6×10^6 hadronic events from 217 pb^{-1} of data which correspond to 9.9×10^5 $\Upsilon(3S)$ decays. Hadronic events are identified by the presence of minimum ionizing tracks in the calorimeter. To reject background events from beam-wall and beam-gas interactions, we also require that the event fire the total-energy trigger and have some energy balance between detector halves. The average observed cluster multiplicity in hadronic events is eleven. On the average six clusters are due to charged particles. About 51% of our hadronic events are due to $\Upsilon(3S)$ decays, the remainder is due to continuum production of lighter quark pairs, $e^+e^- \rightarrow q\bar{q}$.

A clustering algorithm groups all crystal energy depositions into clusters, in order to measure the energy of the showers in the calorimeter. The description given here is necessarily simplified. The algorithm works in several stages. The two polar halves of the detector are first clustered independently. In the first stage the cluster cores are identified by binding together all adjacent crystals with energy depositions of more than 10 MeV in one layer. Then the clusters in different layers which overlap in azimuth are merged. Using this core the clusters are further developed in the second stage so that every crystal with energy of more than 0.3 MeV is assigned to a cluster. Finally, in the third stage, clusters in different polar halves are merged if they are separated by less than

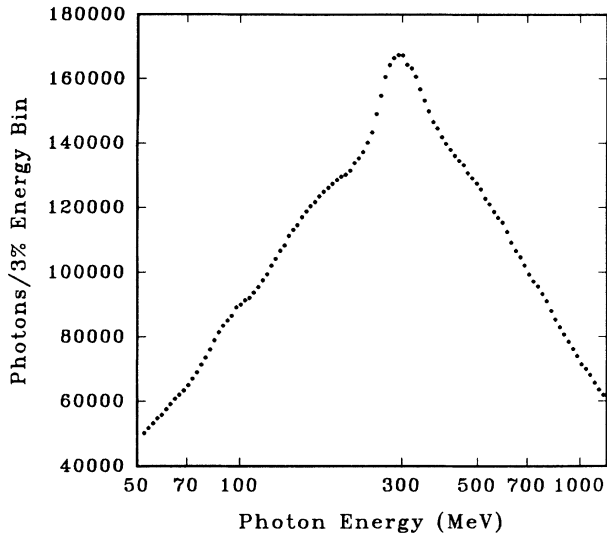


FIG. 1. Energy spectrum of all clusters in hadronic $\Upsilon(3S)$ events.

2.5° in azimuth or by less than 10° if one cluster has five times more energy than the other. Figure 1 shows the energy spectrum of all clusters from hadronic $\Upsilon(3S)$ decays. The broad peak near 300 MeV is due to minimum ionizing particles.

In order to select clusters due to photons and reject minimum ionizing particles, we reject any cluster which contains crystals from a sector with track quality $Q > 1$. To reject charged particles we veto all clusters to which a drift chamber track is pointing. This eliminates electrons and positrons which also give rise to electromagnetic showers. To improve the energy resolution we require photon candidates to be well isolated, i.e., that the largest energy in a crystal adjacent to any crystal of the cluster is less than 2% of the cluster energy and the sum of the energies in all crystals adjacent to the cluster is less than 9% of the cluster energy. Fast charged hadrons are typically much more penetrating than electromagnetic showers and rejected by allowing at most 10% of the cluster energy in NaI and not more than 2 MeV in lead glass. For photon candidates we require the rms width of the cluster to be less than 5.5° and a good match between energy weighted azimuths of the individual layers of the cluster. Finally we test the shower shape by calculating the quantity

$$\zeta = \sum_{i=1}^n \sum_{j=1}^n (E_i - \bar{E}_i) G_{ij}^{-1} (E_j - \bar{E}_j), \quad (4.1)$$

where E_i is the fraction of the cluster energy deposited in crystal i , and n the total number of crystals of the cluster. The average crystal energies \bar{E}_i and the covariance matrix G are obtained from Monte Carlo-generated photons. The matrix elements G_{ij} are given by

$$G_{ij} = \frac{1}{N} \sum_{m=1}^N (E_i - \bar{E}_i)(E_j - \bar{E}_j), \quad (4.2)$$

which is constructed using a total of N Monte Carlo photons [4]. This criterion is designed to recognize clean

photons based on the shower energy profile in the calorimeter. The distribution of the covariance variable ζ is similar to a χ^2 distribution and independent of the incident particle energy. Figure 2 shows the inclusive photon spectrum after all the above shape cuts have been applied. Now the spectral lines due to transitions within the $b\bar{b}$ system have emerged on top of the background.

We predict the shape of the background using the inclusive photon spectra from data taken at the $\Upsilon(1S)$ energy and on the continuum at a beam energy of 5.26 GeV. We characterize the event topology by a planar thrust variable:

$$T = \max_n \left[\frac{\sum_i E_i |\cos \phi_{i,n}|}{\sum_i E_i} \right]. \quad (4.3)$$

The sum index i runs over all 36 BGO sectors, n is the sector for which the sum has its largest value, $\phi_{i,n}$ is the azimuthal angle between sectors i and n , and E_i is the energy in sector i . Events which proceed through $q\bar{q}$ intermediate states are 2-jet-like and have higher thrust than the 3-jet-like ggg events. At the $\Upsilon(3S)$ there is also some contribution from gg and $q\bar{q}g$ intermediate states due to χ_b decays. Because of the geometry of our detector, gg events look very much like $q\bar{q}$ events. The gluon in $q\bar{q}g$ events is soft, so that these states also essentially look like $q\bar{q}$ states. In order to determine the relative proportion of 2-jet and 3-jet-like events present in the $\Upsilon(3S)$ data set we perform a fit of a linear combination of the planar thrust distribution from data taken at the $\Upsilon(1S)$ energy and continuum data to that of data taken at the $\Upsilon(3S)$ energy. The relative contribution of the two distributions is the only free parameter. We find that a combination of $(50.8 \pm 0.3)\%$ $\Upsilon(1S)$ data and the balance continuum data gives the best fit.

This implies that a $(22.7 \pm 0.7)\%$ continuum admixture to the thrust spectrum of $\Upsilon(1S)$ decays is needed to represent the thrust spectrum of $\Upsilon(3S)$ decays. Here we

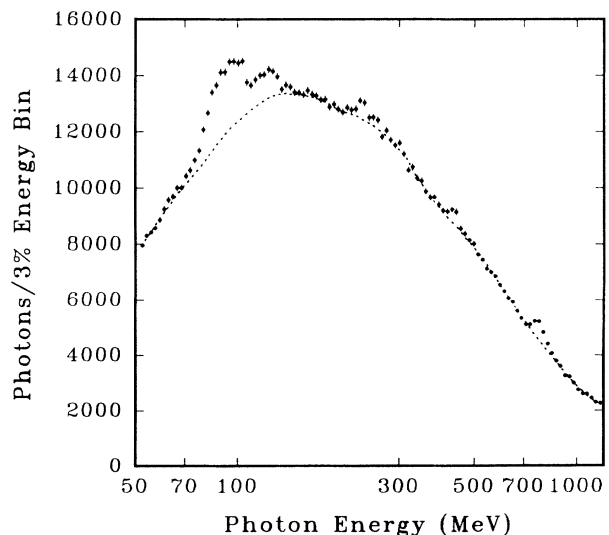


FIG. 2. Inclusive photon spectrum at $\Upsilon(3S)$ and predicted background.

used that 77.0% of the hadronic events at the $\Upsilon(1S)$ energy and 50.6% at the $\Upsilon(3S)$ are due to resonance decays. This additional high thrust component is due to hadronic decays of χ_b states, which are not present in the $\Upsilon(1S)$ data. Assuming that gg and $q\bar{q}g$ final states have the same thrust distribution as continuum events, the excess high thrust component directly measures the fraction of hadronic $\Upsilon(3S)$ decays which proceed via $\chi_b \rightarrow gg$ or $\chi_b \rightarrow q\bar{q}g$. We correct the fitted number for the contributions due to $\chi_b(1P)$ decays and normalize to the total number of $\Upsilon(3S)$ decays. In this way we measure

$$\sum_J B(\Upsilon(3S) \rightarrow \chi_b(2P_J) \rightarrow gg, q\bar{q}g) = (20.2 \pm 0.7)\% . \quad (4.4)$$

The error is statistical only, systematic errors due to $\tau^+\tau^-$ and γgg events are expected to be of the same order of magnitude. This is in good agreement with the CUSB-I measurement [5] and our results from the exclusive and inclusive analyses, given below. This demonstrates that $q\bar{q}$ events are indeed a good model for gg and $q\bar{q}g$ events in our detector. Figure 3 shows the thrust distributions from $\Upsilon(3S)$ data (points) and $\Upsilon(1S)$ data (dotted line). The dashed line is the distribution from continuum events and the solid line is the fitted sum of the $\Upsilon(1S)$ and continuum distributions.

The so constructed background spectrum is normalized to the number of $\Upsilon(3S)$ hadronic events. The contribution of $\pi^0\pi^0$ transitions between Υ states to the background is modeled by adding Monte Carlo-generated π^0 's to hadronic events obtained from $\Upsilon(1S)$ data. These events are then analyzed in the same way as the data. The size of the contribution due to these transitions is determined using the measured branching ratios [6]. The predicted background is shown as a dashed line in Fig. 2, superimposed on the inclusive photon spectrum at the $\Upsilon(3S)$ energy.

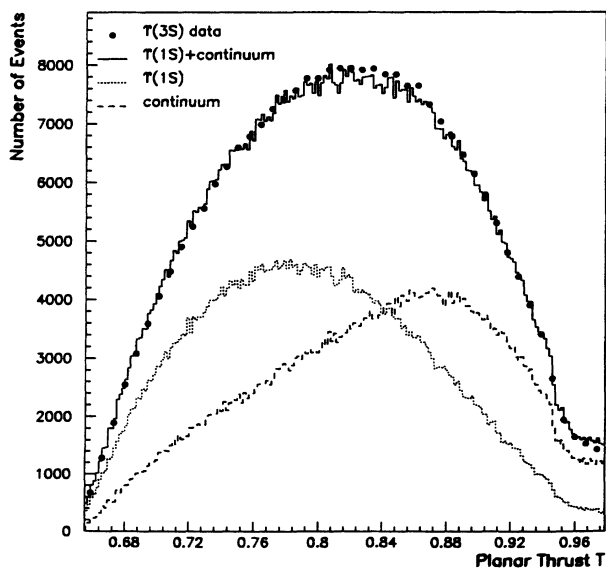


FIG. 3. Planar thrust distribution from $\Upsilon(3S)$, $\Upsilon(1S)$, and continuum data. The curves are explained in the text.

Figure 4 shows the inclusive photon spectrum at the $\Upsilon(3S)$ after subtraction of the predicted background. The superimposed curves are a fit to the data, representing each of the 24 allowed electric dipole transitions by a detector resolution function. The parameters of the fit and the curves as they are numbered in Fig. 4 are explained in the following.

(1) $\Upsilon(3S) \rightarrow \chi_b(2P_J)\gamma$. All three peak positions and areas are free parameters.

(2) $\chi_b(2P_J) \rightarrow \Upsilon(2S)\gamma$. The average peak position and the total area are free parameters, the splitting is fixed to be the same as for the three peaks in point (1) and the relative intensities are determined by the product branching ratios $B(\Upsilon(3S) \rightarrow \chi_b(2P_J)\gamma) \times B(\chi_b(2P_J) \rightarrow \Upsilon(2S)\gamma)$, measured in the exclusive channel.

(3) $\chi_b(2P_J) \rightarrow \Upsilon(1S)\gamma$. Analogous to point (2).

(4) $\Upsilon(3S) \rightarrow \chi_b(1P_J)\gamma$. The average peak position and the total area are free, the splitting is fixed by previous measurements [6] and the relative intensities are determined by spin and phase space factors for electric dipole transitions: $(2J+1)E_\gamma^3$.

(5) $\chi_b(1P_J) \rightarrow \Upsilon(1S)\gamma$. All parameters are fixed by previous measurements [6,7] and the intensities of the feeding transition in point (4).

(6) $\Upsilon(2S) \rightarrow \chi_b(1P_J)\gamma$. All parameters are fixed by previous measurements [6].

(7) $\chi_b(2P_J) \rightarrow \Upsilon(1D)\gamma$ and $\Upsilon(1D) \rightarrow \chi_b(1P_J)\gamma$. All parameters fixed to predictions of Ref. [8]. The spectrum is consistent with the predictions. The minimum value of χ^2 increases by 0.7 without any D state signal.

Table I lists the fitted values for the 12 free parameters of the fit. The errors quoted are statistical only. We can estimate systematic effects on the fitted energies of the photon lines, which may be due to the incomplete resolution of the 87 and 100 MeV lines in the inclusive spectrum, by comparing the energies to the result from the fit

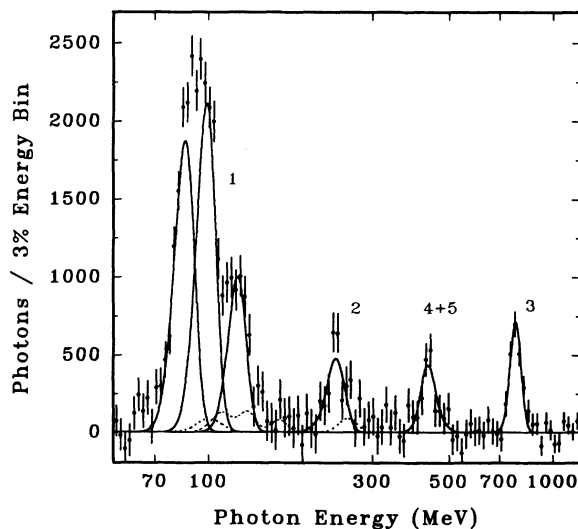


FIG. 4. Background subtracted inclusive photon spectrum at $\Upsilon(3S)$. The superimposed curves are a fit to the data. See text for explanation of the curves. The dashed curve corresponds to point (6), the dotted curves to point (7) in the text.

TABLE I. Results of fit to background-subtracted spectrum. Energy scale errors (0.9%) are not included.

Transition	E_γ (MeV)	Events
$\Upsilon(3S) \rightarrow \chi_b(2P_2)\gamma$	86.7 ± 0.4	$10\,319 \pm 478$
$\Upsilon(3S) \rightarrow \chi_b(2P_1)\gamma$	100.1 ± 0.4	$11\,147 \pm 462$
$\Upsilon(3S) \rightarrow \chi_b(2P_0)\gamma$	123.0 ± 0.8	4959 ± 339
$\chi_b(2P) \rightarrow \Upsilon(2S)\gamma$	236.1 ± 2.6	2429 ± 332
$\chi_b(2P) \rightarrow \Upsilon(1S)\gamma$	770.3 ± 2.9	1994 ± 150
$\Upsilon(3S) \rightarrow \chi_b(1P)\gamma$	446.9 ± 2.9	1163 ± 168

to the exclusive spectrum (see Table IV), in which the photon lines are completely resolved. The good agreement of the energies from both spectra suggests that systematic effects are small compared to statistical errors. The CLEO Collaboration has recently reported values for the energies of the transition photons, which are in good agreement with our results [9].

The calibration of the absolute energy scale is checked by comparing the measured sum of photon energies in exclusive events of the type $\Upsilon(3S) \rightarrow \chi_b(2P_J)\gamma \rightarrow \Upsilon\gamma\gamma$ with their nominal value, derived from the well measured masses of the Υ states. The peak positions also vary slightly as a function of the photon selection cuts. We estimate the overall systematic uncertainty on the energy scale to be 0.9%.

To determine the detector response for inclusive events, Monte Carlo generated photons were added to real hadronic events. These events were analyzed by the same programs which were used for the data. Figure 5 shows the measured energy distribution for 85 MeV Monte Carlo photons. The superimposed curve is a fit to the data. We find that a double Gaussian describes the detector response well. The smaller one of the two Gaussians is slightly displaced towards a lower energy

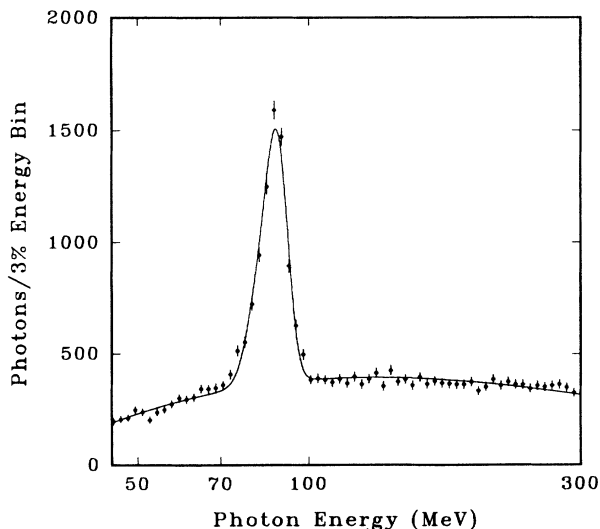


FIG. 5. Detector response to 85 MeV Monte Carlo photons.

and has one third the area of the larger one. We find that the width σ of the Gaussians varies as a function of their mean E_γ according to $\sigma/E_\gamma = \kappa/(E_\gamma/1 \text{ GeV})^{1/4}$. The parameter κ depends on the clustering algorithm. For the present analysis $\kappa = (3.1 \pm 0.2)\%$. The dependence of κ on the event topology is negligible. We obtain $\kappa = (3.17 \pm 0.15)\%$ from Monte Carlo photons superimposed on $\Upsilon(1S)$ events and $\kappa = (3.04 \pm 0.07)\%$ from Monte Carlo photons superimposed on continuum events.

The Monte Carlo photons were generated using the EGS program [10]. A more detailed description of the CUSB Monte Carlo simulation can be found elsewhere [3]. We have checked how well the Monte Carlo simulation reproduces the detector response by comparing the energy spectra of Monte Carlo photons with the energy spectrum of photons from exclusive events. Their shapes are in good agreement. We also compared 5 GeV Monte Carlo electrons and real electrons from Bhabha scattering events and find good agreement.

The efficiency for a given transition is the product of the efficiency to detect the event as a hadronic event and the efficiency for finding the photon in a hadronic event. These efficiencies depend on event topology. The final state topology is either 2-jet like in the case of $q\bar{q}, gg$, and $q\bar{q}g$ final states, or 3-jet like in the case of ggg final states.

To determine the photon finding efficiencies we use continuum data to simulate 2-jet-like events. To simulate 3-jet-like events we use $\Upsilon(1S)$ data and statistically subtract the continuum contribution. It is easier to find photons in 2-jet-like events which have a smaller observed multiplicity than in busier 3-jet-like events. On the other hand, the acceptance of the detector is larger for 3-jet-like events resulting in a higher hadronic efficiency. To determine the hadronic efficiency of the detector we use a Monte Carlo simulation. For 2-jet-like events we find $(82.7 \pm 0.9)\%$, for 3-jet-like events $(89.2 \pm 0.9)\%$. The photon finding efficiency is obtained by adding Monte Carlo photons to real hadronic events. The photons have been generated with an angular distribution which was calculated assuming pure electric dipole transitions [11]. We combine these efficiencies in the correct proportion of 2- and 3-jet-like events for the individual decay chains. For the transitions $\Upsilon(3S) \rightarrow \chi_b(2P_J)\gamma$ the overall efficiencies are 9.4%, 9.9%, and 8.5% for $J=2, 1, 0$ with an error of 4% of their value. For the transition $\chi_b(2P) \rightarrow \Upsilon(2S)\gamma$ the efficiency is $(5.5 \pm 0.7)\%$ and for $\chi_b(2P) \rightarrow \Upsilon(1S)\gamma$ it is $(9.9 \pm 0.8)\%$.

From the fitted areas in Table I and these efficiencies we find the branching ratios of the various transitions listed in Table II. The total branching ratio reported by CLEO [9] is in agreement with ours. Whenever two errors are quoted, the first one is statistical and the second one systematic. The fitted area of the signal at 450 MeV together with the previously measured [6] branching ratios for the transitions $\Upsilon(3S) \rightarrow \Upsilon(2S) + X$, $\Upsilon(2S) \rightarrow \chi_b(1P)\gamma$, $\chi_b(1P) \rightarrow \Upsilon(1S)\gamma$ leads to the product branching ratio

$$\sum_J B(\Upsilon(3S) \rightarrow \chi_b(1P_J)\gamma) B(\chi_b(1P_J) \rightarrow \Upsilon(1S)\gamma) = (1.7 \pm 0.4 \pm 0.6) \times 10^{-3}. \quad (4.5)$$

TABLE II. Branching ratios from inclusive analysis.

Transition	B (%)
$\Upsilon(3S) \rightarrow \chi_b(2P_2)\gamma$	$11.1 \pm 0.5 \pm 0.4$
$\Upsilon(3S) \rightarrow \chi_b(2P_1)\gamma$	$11.5 \pm 0.5 \pm 0.5$
$\Upsilon(3S) \rightarrow \chi_b(2P_0)\gamma$	$6.0 \pm 0.4 \pm 0.6$
$\Upsilon(3S) \rightarrow \chi_b(2P)\gamma \rightarrow \Upsilon(2S)\gamma\gamma$	$4.2 \pm 0.6 \pm 0.5$
$\Upsilon(3S) \rightarrow \chi_b(2P)\gamma \rightarrow \Upsilon(1S)\gamma\gamma$	$2.0 \pm 0.2 \pm 0.2$

Using the total width of the $\Upsilon(3S)$ of (24.3 ± 2.9) keV [6], together with the measured branching ratios from Table II we derive the absolute rates of the transitions $\Upsilon(3S) \rightarrow \chi_b(2P_J)\gamma$. These transitions are allowed electric dipole transitions and their rates are given by

$$\Gamma_{E1}(^3S_1 \rightarrow ^3P_J + \gamma) = \frac{4}{27} \alpha e_q^2 E_\gamma^3 (2J+1) |\langle r_{fi} \rangle|^2, \quad (4.6)$$

where α is the fine-structure constant, e_q the quark charge in units of the electron charge, and E_γ the energy of the photon. The dipole matrix element $\langle r_{fi} \rangle$ is defined as

$$\langle r_{fi} \rangle = \int_0^\infty R_f(r) r R_i(r) r^2 dr \quad (4.7)$$

and can be evaluated using the wave functions of the initial and final states, R_i and R_f , given by potential models. In Table III the measured rates are compared with values calculated using our measured photon energies and the electric dipole matrix elements given by Gupta, Radford, and Repko (GRR) [12], Moxhay and Rosner (MR) [13], McClary and Byers (MB) [14], Kwong and Rosner (KR) [8], Franzini (PF) [15], and Fulcher (LF) [16].

The agreement between experiment and theory is excellent, indicating that potential models describe the spin-independent features of the $b\bar{b}$ system well. The electric dipole rates are proportional to $E_\gamma^3(2J+1)$. Therefore, the excellent agreement between the experimental values and the model calculations confirm the spin assignment for the $\chi_b(2P_J)$ states.

We have modified the previously described fit to search for a monochromatic photon signal around 480 MeV from the cascade $\Upsilon(3S) \rightarrow h_b \pi \pi \rightarrow \eta_b \gamma \pi \pi$. We add an additional detector response function and vary its mean and area to minimize χ^2 . For a hyperfine splitting between $\Upsilon(1S)$ and η_b of (50–110) MeV [17] we obtain a 90% confidence level upper limit for the product branching ratio $B(\Upsilon(3S) \rightarrow h_b \pi \pi) \times B(h_b \rightarrow \eta_b \gamma)$ of 0.45%.

TABLE III. Transition rates for $\Upsilon(3S) \rightarrow \chi_b(2P_J)\gamma$ in keV.

J	Experiment	GRR	MR	MB	KR	PF	LF
2	$2.7 \pm 0.1 \pm 0.3$	2.6	3.0	2.8	2.8	2.8	2.7
1	$2.8 \pm 0.1 \pm 0.4$	2.4	2.6	2.2	2.6	2.6	2.5
0	$1.5 \pm 0.1 \pm 0.2$	1.5	1.5	1.0	1.6	1.6	1.6
Σ	$7.0 \pm 0.2 \pm 0.5$	6.5	7.1	6.0	7.0	7.0	6.8

The product branching ratio for this transition is expected to be between 0.05% and 0.5% [18].

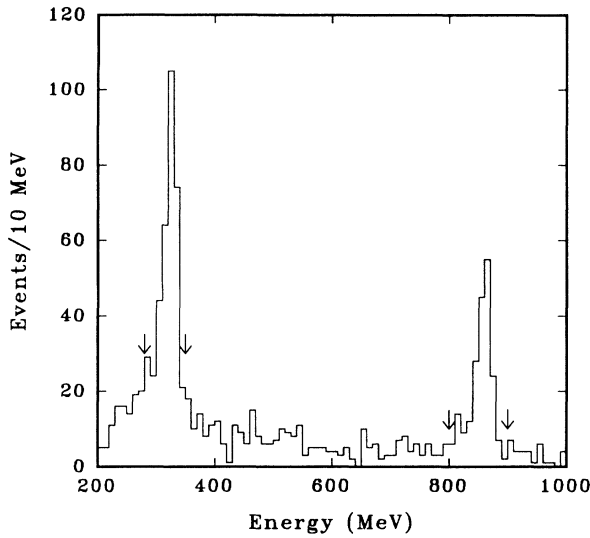
V. EXCLUSIVE EVENTS

Events due to the reaction $\Upsilon(3S) \rightarrow \chi_b \gamma \rightarrow \Upsilon \gamma \gamma$, followed by $\Upsilon \rightarrow \mu^+ \mu^-$ or $\Upsilon \rightarrow e^+ e^-$ can be identified with very little background by selecting events with two photons and a nearly collinear muon or electron-positron pair. Since the complete event is reconstructed we call these events “exclusive” events.

The data is first scanned by computer to perform a preliminary clustering of the energy depositions. The events are selected using the selection criteria described below. The accepted events are then examined by physicists who revise the clustering if necessary. Then all cluster parameters are recalculated using the revised clustering and the selection criteria are applied again.

For events in which leptons from the decay of the final Υ state are detected in the calorimeter we distinguish between events with an electron-positron pair ($ee\gamma\gamma$ events) and events with a muon pair ($\mu\mu\gamma\gamma$ events). If the leptons fire the end-cap trigger ($end\text{-}cap \gamma\gamma$ events) we cannot distinguish between muons and electrons. We shall refer to all these events together as $ll\gamma\gamma$ events. For $\mu\mu\gamma\gamma$ events we require either a total energy, two-muon or distributed energy trigger, $200 \text{ MeV} < E_{\text{BGO}} < 1.5 \text{ GeV}$, $E_{\text{BGO}} + E_{\text{NaI}} < 2 \text{ GeV}$, and two minimum ionizing tracks in BGO or NaI, collinear within 15° in φ . E_{BGO} is the total energy deposited in BGO, E_{NaI} the total energy deposited in NaI, φ the azimuthal angle. For $ee\gamma\gamma$ events we require a total energy trigger, $9.3 \text{ GeV} < E_{\text{BGO}} + E_{\text{NaI}} < 10.7 \text{ GeV}$, and that the two most energetic showers are collinear within 15° in φ . For $end\text{-}cap \gamma\gamma$ events the pulse heights for the two leptons in the end-cap scintillators have to be greater than 75% of the pulse height expected for minimum ionizing particles. In addition, for all events we require that there are two photons with energies between 50 MeV and 1 GeV and no additional tracks or clusters above 15 MeV in the calorimeter. A cluster is called a photon if more than half its energy is in BGO, but less than 80% of its energy in the first layer of BGO, less than 50%–90% of its energy, depending on photon energy, is in a single crystal, its energy weighted width is less than 7° , and no drift chamber track is within 20° in φ of the photon. The width is defined as $\sum_i E_i |\varphi_i - \varphi_\gamma| / E_\gamma$, where the sum runs over all crystals of the cluster and E_i is the energy in crystal i , φ its central azimuth, E_γ the energy of the cluster and φ_γ its energy weighted azimuth. For every event we require at least one well isolated photon, for which the sum of the energies of all adjacent crystals is less than 5% of the photon energy.

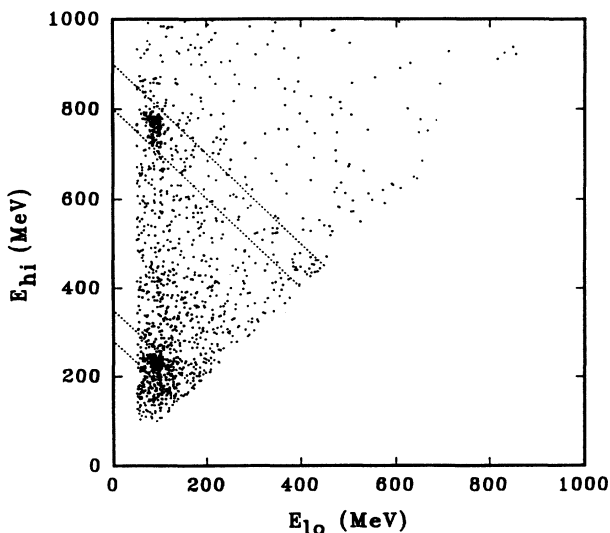
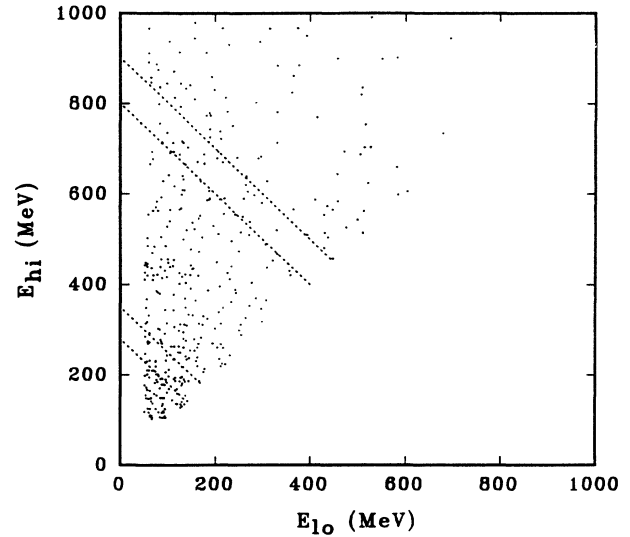
The data sample is based on 1.32×10^6 $\Upsilon(3S)$ decays for $ee\gamma\gamma$ events, 1.18×10^6 $\Upsilon(3S)$ decays for $\mu\mu\gamma\gamma$ events, and 6.2×10^5 $\Upsilon(3S)$ decays for $end\text{-}cap \gamma\gamma$ events. Figure 6 shows the spectrum of the sum of the two photon energies (E_{sum}) of all $ll\gamma\gamma$ events. The two peaks at 330 MeV, consistent with the mass difference between $\Upsilon(3S)$ and $\Upsilon(2S)$, and 860 MeV, consistent with the mass difference between $\Upsilon(3S)$ and $\Upsilon(1S)$, confirm that the

FIG. 6. Sum of photon energies in $ll\gamma\gamma$ events.

events are due to transitions between these states.

Figure 7 shows a scatter plot of the energy of the lower energy photon (E_{l_0}) versus the energy of the higher energy photon (E_{hi}). The data points cluster in two places, as expected for the two cascades. The lower energy photon comes from the process $\Upsilon(3S) \rightarrow \chi_b(2P)\gamma$, the higher energy photon from $\chi_b(2P) \rightarrow \Upsilon(1S)\gamma$ or $\chi_b(2P) \rightarrow \Upsilon(2S)\gamma$. Both clusters split into vertical bands due to the fine structure of the $\chi_b(2P)$ states.

We have searched for $ll\gamma\gamma$ events in data taken on the continuum at a beam energy of 5.26 GeV. In the corresponding scatter plot, which is given in Fig. 8, we do not observe any clustering of the data points. However, the continuum production of $ll\gamma\gamma$ events due to initial- and final-state radiation is a source of background for the

FIG. 7. Scatter plot of E_{l_0} versus E_{hi} for $ll\gamma\gamma$ events.FIG. 8. Scatter plot for $ll\gamma\gamma$ events from continuum data.

$\Upsilon(3S)$ data sample. This background is strongest for the $ee\gamma\gamma$ mode. The $\mu\mu\gamma\gamma$ channel is much cleaner since the probability for muons to radiate a photon is much smaller. A second source of background is the process $\Upsilon(3S) \rightarrow \Upsilon(1S)\pi^0\pi^0$, where only two of the four photons from the decay of the π^0 's are detected. Their contribution however is much smaller than the continuum background.

To reject background we only accept events in the two peaks of the E_{sum} spectrum. We cut at $280 \text{ MeV} < E_{\text{sum}} < 350 \text{ MeV}$ for $\Upsilon(2S)$ final states and $800 \text{ MeV} < E_{\text{sum}} < 900 \text{ MeV}$ for $\Upsilon(1S)$ final states. These cuts are indicated by the arrows in Fig. 6 and the diagonal lines in Fig. 7.

Figure 9 shows the spectrum of E_{l_0} of the events in the

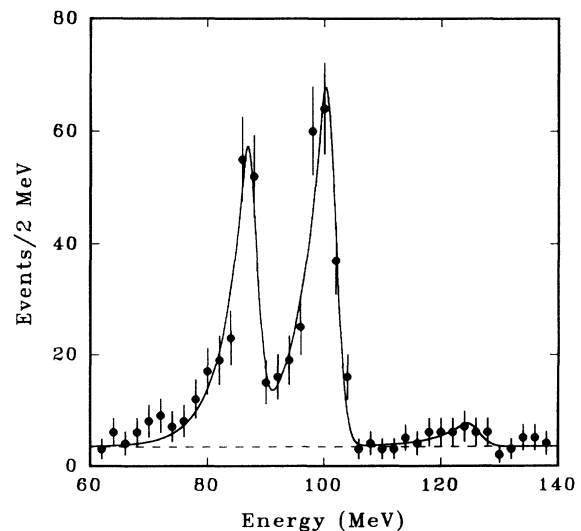
FIG. 9. Spectrum of E_{l_0} in $ll\gamma\gamma$ events.

TABLE IV. Results of fit to the spectrum of $E_{i\bar{b}}$ from $ll\gamma\gamma$ events. Energy scale errors are not included.

Spin of χ_b	E_γ (MeV)	N	N_{2S}	N_{1S}
2	86.9 ± 0.4	157 ± 15	87 ± 11	89 ± 10
1	100.2 ± 0.5	223 ± 17	125 ± 13	100 ± 12
0	124.6 ± 1.4	17 ± 7	10 ± 6	5 ± 3

two signal regions. Two well resolved lines are visible above a small background. The third line is expected to be suppressed because of the large hadronic width expected for the $\chi_b(2P_0)$ state. The curve is a fit to the data, assuming the presence of three spectral lines and a background of 3.0 ± 0.3 events per 2 MeV bin. The background level has been determined from the continuum data and a Monte Carlo simulation of the $\pi^0\pi^0$ transitions. Each line is represented by a Gaussian with an exponential low-energy tail to describe the detector response for exclusive events. The positions and areas of the three lines and the width of the response function are free parameters of the fit. The fitted width of the lines is 2 MeV at a peak position of 100 MeV. The fitted values of positions (E_γ) and areas (N) are listed in Table IV. We also give the areas (N_{2S}, N_{1S}) from separate fits to the spectra from events of the $\Upsilon(2S)$ and $\Upsilon(1S)$ signal regions.

To estimate acceptance \times efficiency (ϵ) of the selection process, we have analyzed a sample of Monte Carlo events in the same way as the data. The events were generated with an angular distribution, calculated under the assumption of pure electric dipole transitions [11]. Table V lists the values for ϵ . In the sample of events from the $\Upsilon(2S)$ signal region there is a small contribution from events in which the $\Upsilon(2S)$ state did not decay leptonically but to $\Upsilon(1S) + X$, followed by a leptonic $\Upsilon(1S)$ decay. If X escapes detection these events look like genuine $ll\gamma\gamma$ events. The observed number of events has to be corrected down by 7% due to this effect.

Assuming lepton universality and using the measured branching ratios of the final Υ states into muons, $B_{\mu\mu}(1S) = (2.57 \pm 0.07)\%$ [6] and $B_{\mu\mu}(2S) = (1.44 \pm 0.10)\%$ [19], we calculated the product branching ratios given in Table VI. We have used $B(\Upsilon(3S) \rightarrow \chi_b(2P_J)\gamma)$ from Table II to derive the values of $B(\chi_b(2P_J) \rightarrow \Upsilon\gamma)$.

In the region of the scatter plot in Fig. 7 where both photons have energies of about 430 MeV we see an excess of events. This signal is clearly visible in the energy spectrum of all photons of events in the $\Upsilon(1S)$ signal region

[20]. The photon energies are consistent with the transition $\Upsilon(3S) \rightarrow \chi_b(1P_{J=1,2})\gamma \rightarrow \Upsilon(1S)\gamma\gamma$. To determine the significance of this excess we perform a maximum likelihood calculation using Poisson statistics. From Monte Carlo simulation we obtain the expected distribution of events from the transition $\Upsilon(3S) \rightarrow \chi_b(1P)\gamma \rightarrow \Upsilon(1S)\gamma\gamma$. We estimate the background from the surrounding region of the scatter plot. We find that it would be a 4.5σ effect for this background to fluctuate up to the level of the observed signal. The likelihood function has its maximum at a signal of $15.1^{+5.2}_{-4.4}$ events. Acceptance \times efficiency are determined from a Monte Carlo calculation to be $\epsilon = (13.7 \pm 1.0)\%$ for $ee\gamma\gamma$ events and $\epsilon = (17.7 \pm 0.5)\%$ for $\mu\mu\gamma\gamma$ events. The observed number of events corresponds to a product branching ratio

$$\sum_{J=1,2} B(\Upsilon(3S) \rightarrow \chi_b(1P_J)\gamma) B(\chi_b(1P_J) \rightarrow \Upsilon(1S)\gamma) = (1.2^{+0.4}_{-0.3} \pm 0.09) \times 10^{-3}. \quad (5.1)$$

This measurement is in agreement with the value extracted from the fit to the inclusive photon spectrum.

The electric dipole matrix elements for the transition $\Upsilon(3S) \rightarrow \chi_b(1P)\gamma$ are extremely sensitive to relativistic corrections. Owing to the different numbers of nodes in the radial wave functions of initial and final states, large cancellations, which are very sensitive to small corrections to the wave functions, can occur in the integral in Eq. (4.7). There is a range of calculated values for this matrix element. We convert these into predictions for the product branching ratio using the measured width of the $\Upsilon(3S)$ and $B(\chi_b(1P) \rightarrow \Upsilon(1S)\gamma)$ [6]. The nonrelativistic calculation of Eichten *et al.* [21] gives a product branching ratio of 11.2×10^{-3} , other authors obtain 1.7×10^{-3} (MR) [13], 1.5×10^{-3} (GRR) [12], 0.49×10^{-3} (KR) [8], and 0.44×10^{-3} (PF) [15]. Our measurement agrees best with the models of MR and GRR which include relativistic corrections.

We searched the exclusive event sample for events which are consistent with the double cascade $\Upsilon(3S) \rightarrow \chi_b(2P_J)\gamma \rightarrow \Upsilon(1D_{J'})\gamma\gamma$, $\Upsilon(1D_{J'}) \rightarrow \chi_b(1P_{J''})\gamma \rightarrow \Upsilon(1S)\gamma\gamma$, $\Upsilon(1S) \rightarrow e^+e^-$ or $\mu^+\mu^-$. Kwong and Rosner [8] predict a product branching ratio, summed over all intermediate spins of 0.14% for this double cascade. For the $\Upsilon(1^3D_J)$ states with $J=1,2,3$ they predict masses of 10 150 MeV, 10 156 MeV, and 10 160 MeV. We select events with exactly four photons and then compare the measured photon energies with their nominal energies obtained using the predicted masses of the $\Upsilon(1^3D_J)$ states. We find one such event for

TABLE V. Efficiencies for $ll\gamma\gamma$ events (%).

	$\Upsilon(3S) \rightarrow \chi_b(2P_J)\gamma \rightarrow \Upsilon(1S)\gamma\gamma$			$\Upsilon(3S) \rightarrow \chi_b(2P_J)\gamma \rightarrow \Upsilon(2S)\gamma\gamma$		
	$J=0$	$J=1$	$J=2$	$J=0$	$J=1$	$J=2$
$\mu\mu\gamma\gamma$	14.3 ± 0.5	16.6 ± 0.5	13.9 ± 0.5	11.9 ± 0.5	13.2 ± 0.5	10.7 ± 0.5
$ee\gamma\gamma$	9.4 ± 0.4	10.6 ± 0.4	8.5 ± 0.4	10.3 ± 0.4	12.7 ± 0.4	10.6 ± 0.4
<i>end-cap</i> $\gamma\gamma$	3.0 ± 0.2	3.9 ± 0.2	3.8 ± 0.2	2.5 ± 0.2	3.6 ± 0.2	3.1 ± 0.2

TABLE VI. Branching ratios from exclusive analysis.

J	$B(\Upsilon(3S) \rightarrow \chi_b(2P_J)\gamma \rightarrow \Upsilon(2S)\gamma\gamma)$	$B(\chi_b(2P_J) \rightarrow \Upsilon(2S)\gamma)$
2	$(1.90 \pm 0.23 \pm 0.18)\%$	$(17.3 \pm 2.1 \pm 1.9)\%$
1	$(2.29 \pm 0.23 \pm 0.21)\%$	$(19.9 \pm 2.0 \pm 2.2)\%$
0	$(0.28 \pm 0.12 \pm 0.03)\%$	$(4.6 \pm 2.0 \pm 0.7)\%$
J	$B(\Upsilon(3S) \rightarrow \chi_b(2P_J)\gamma \rightarrow \Upsilon(1S)\gamma\gamma)$	$B(\chi_b(2P_J) \rightarrow \Upsilon(1S)\gamma)$
2	$(0.77 \pm 0.11 \pm 0.05)\%$	$(7.0 \pm 1.0 \pm 0.6)\%$
1	$(0.91 \pm 0.11 \pm 0.06)\%$	$(8.0 \pm 0.9 \pm 0.7)\%$
0	$(0.05 \pm 0.04 \pm 0.01)\%$	$(0.9 \pm 0.6 \pm 0.1)\%$

which the measured photon energies are consistent with the double cascades $\Upsilon(3S) \rightarrow \chi_b(2P_1)\gamma \rightarrow \Upsilon(1D_1)\gamma\gamma \rightarrow \chi_b(1P_2)\gamma\gamma\gamma \rightarrow \Upsilon(1S)\gamma\gamma\gamma\gamma$ and $\Upsilon(3S) \rightarrow \chi_b(2P_1)\gamma \rightarrow \Upsilon(2S)\gamma\gamma \rightarrow \chi_b(1P_2)\gamma\gamma\gamma \rightarrow \Upsilon(1S)\gamma\gamma\gamma\gamma$. This translates into a 90% confidence level upper limit of 2.8×10^{-3} on the product branching ratio for the double cascade through the $\Upsilon(1D_J)$ states. This is twice the prediction of Kwong and Rosner and more data is therefore needed to test this prediction.

VI. FINE STRUCTURE OF THE $\chi_b(2P)$ STATES

The fine structure of the $\chi_b(2P)$ states give information about the spin dependence of the interquark potential. Asymptotic freedom implies that at short distances the interquark interaction is dominated by single-gluon (vector) exchange. At large distances the interaction is mediated by the exchange of many gluons and the Lorentz nature of the effective coupling has not been derived from first principles. Lattice calculations [22] and many potential model calculations favor the exchange of an effective scalar system. As we shall see, our measurement of the fine structure of the $\chi_b(2P)$ states supports this choice.

If we write the interquark potential as the sum of a part due to vector exchange (V_V) and a part due to scalar exchange (V_S), the spin-dependent terms of the Hamiltonian can be written as

$$\begin{aligned}
V(r) = & \frac{1}{2m_b^2 r} \mathbf{L} \cdot \mathbf{S} \left[3 \frac{d}{dr} V_V - \frac{d}{dr} V_S \right] \\
& + \frac{S_{12}}{12m_b^2} \left[\frac{1}{r} \frac{d}{dr} V_V - \frac{d^2}{dr^2} V_V \right] \\
& + \frac{2}{3m_b^2} \mathbf{S}_1 \cdot \mathbf{S}_2 \nabla^2 V_V, \quad (6.1)
\end{aligned}$$

where \mathbf{L} is the orbital angular momentum, $\mathbf{S} = \mathbf{S}_1 + \mathbf{S}_2$, $S_{12} = 2(3\hat{\mathbf{r}} \cdot \mathbf{S}_1 \hat{\mathbf{r}} \cdot \mathbf{S}_2 - \mathbf{S}_1 \cdot \mathbf{S}_2)$, and \mathbf{S}_1 and \mathbf{S}_2 are the spins of the constituent quark and antiquark.

In order to compare with measurements we take the following expectation values and parametrize the fine structure in terms of the parameters

$$a = \frac{1}{2m_b^2 r} \left\langle 3 \frac{d}{dr} V_V - \frac{d}{dr} V_S \right\rangle \quad (6.2)$$

for the spin-orbit contribution and

$$b = \frac{1}{12m_b^2} \left\langle \frac{1}{r} \frac{d}{dr} V_V - \frac{d^2}{dr^2} V_V \right\rangle \quad (6.3)$$

for the tensor contribution. Then the masses of the $\chi_b(2P)$ states can be expressed in terms of these two parameters and the spin averaged value $\bar{M}_{\chi_b(2P)}$ as [23]

$$\begin{aligned}
M_{\chi_b(2P_2)} &= \bar{M}_{\chi_b(2P)} + a - \frac{2b}{5}, \\
M_{\chi_b(2P_1)} &= \bar{M}_{\chi_b(2P)} - a + 2b, \\
M_{\chi_b(2P_0)} &= \bar{M}_{\chi_b(2P)} - 2a - 4b.
\end{aligned} \quad (6.4)$$

We define the fine-structure ratio R as

$$R = \frac{M_{\chi_b(2P_2)} - M_{\chi_b(2P_1)}}{M_{\chi_b(2P_1)} - M_{\chi_b(2P_0)}} = \frac{2a - \frac{12}{5}b}{a + 6b}. \quad (6.5)$$

Combining the fitted photon energies from Tables I and IV we obtain $E_\gamma(J=2) = (86.8 \pm 0.3)$ MeV, $E_\gamma(J=1) = (100.1 \pm 0.3)$ MeV, and $E_\gamma(J=0) = (123.4 \pm 0.7)$ MeV. From these energies and the previously measured mass of the $\Upsilon(3S)$ state, we derive the masses of the $\chi_b(2P)$ states. We find $M_{\chi_b(2P_2)} = (10268.1 \pm 0.4 \pm 1.0)$ MeV, $M_{\chi_b(2P_1)} = (10254.7 \pm 0.4 \pm 1.0)$ MeV, and $M_{\chi_b(2P_0)} = (10231.2 \pm 0.8 \pm 1.2)$ MeV. This gives a center of gravity of $\bar{M}_{\chi_b(2P)} = (10259.5 \pm 0.4 \pm 1.0)$ MeV and fine-structure splittings $M_{\chi_b(2P_2)} - M_{\chi_b(2P_1)} = (13.5 \pm 0.4 \pm 0.5)$ MeV and $M_{\chi_b(2P_1)} - M_{\chi_b(2P_0)} = (23.5 \pm 0.7 \pm 0.7)$ MeV. The systematic error on these splittings has been estimated by varying the width of the fitted resolution function and the subtracted background. The values for the parameters a and b and the fine-structure ratio R obtained from these measurements are listed in Table VII. For R we quote three values, one each from the combined photon energies, from the photon energies from exclusive events and from inclusive events separately. We also give the value of the fine-structure ratio for the $\chi_b(1P)$ states, obtained from previous measurements of the $\chi_b(1P)$ fine structure [6]. We compare them to model calculations which differ in their assumptions about the terms in the potential which arise from vector and scalar exchange. Our data confirms the dominance of the spin-orbit force over the tensor force, a common feature of all models. However, numerically our measurements do not agree

TABLE VII. Fine-structure parameters

	Experiment	GRR	MR	MB	PF	LF
a (MeV)	$9.5 \pm 0.2 \pm 0.2$	9.3	6.5	14.6	8.3	10.3
b (MeV)	$2.3 \pm 0.1 \pm 0.1$	1.9	2.1	4.2	1.6	1.9
$R_{\chi_b(2P)}$	$0.574 \pm 0.024 \pm 0.02$	0.67	0.42	0.48	0.71	0.70
Exclusive	$0.544 \pm 0.047 \pm 0.02$					
Inclusive	$0.584 \pm 0.024 \pm 0.02$					
$R_{\chi_b(1P)}$	0.66 ± 0.05	0.64	0.42	0.45	0.70	0.67

well with any of the calculations. Our measurement of $R_{\chi_b(2P)}$ is smaller than $R_{\chi_b(1P)}$, contrary to all model predictions. An improvement in the precision of $R_{\chi_b(1P)}$ is necessary to establish this effect with a higher confidence level, thus leading to a better understanding of the spin-dependent forces.

A possible explanation for this puzzle in the behavior of R has been suggested by Franzini [15]. Potential models predict the mass of the triplet F states of the $b\bar{b}$ system in a range of 0–200 MeV above the mass of the $\chi_b(2P)$ states. Mixing between the $\chi_b(2P_2)$ state and the 1^3F_2 state would lower the mass of the $\chi_b(2P_2)$ state, thus resulting in a smaller value for R . A mixing of 0.04%–0.4%, expressed in terms of the ratio of the off-diagonal term to the diagonal term in the mass matrix, depending on the mass difference between the P and F states is necessary to explain our measured value of $R_{\chi_b(2P)}$.

In order to check whether our measured value of R is consistent with quark confinement by an effective scalar exchange, we make the following ansatz for the interquark potential:

$$V_V = -\frac{4}{3} \frac{\alpha_s}{r} + (1-f)kr, \quad V_S = fkr. \quad (6.6)$$

Then the “scalar fraction” f can be expressed as

$$f = \frac{0.8 + 0.7\lambda - (1 + 0.5\lambda)R}{(0.95 - 0.625R)\lambda}, \quad (6.7)$$

where

$$\lambda = \frac{k}{\alpha_s} \frac{\langle r^{-1} \rangle}{\langle r^{-3} \rangle}. \quad (6.8)$$

The parameter λ can be determined by potential models. In Fig. 10 f is plotted as a function of k/α_s for the $\chi_b(2P)$ and $\chi_b(1P)$ states, using $\langle r^{-1} \rangle / \langle r^{-3} \rangle = 1.2$ for $\chi_b(1P)$ and 1.1 for $\chi_b(2P)$ [8]. We also plot the average of the two curves, which varies between 0.9 and 1.3 for values of k/α_s between 0.5 and 1.5, the range preferred by potential models. This is consistent with $f=1$, corresponding to a confining potential due to scalar exchange.

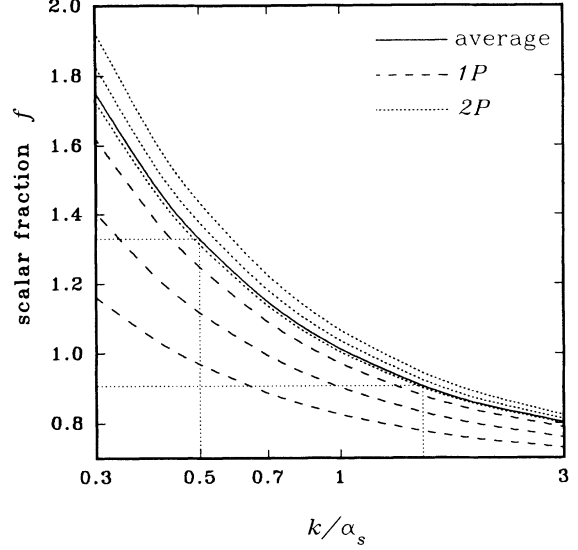


FIG. 10. Scalar fraction of the long-range potential.

VII. HADRONIC WIDTHS OF THE $\chi_b(2P)$ STATES

The annihilation widths of P -wave quarkonium states have been calculated in perturbative QCD, assuming that the annihilation amplitude factorizes into a part describing the bound state and another part describing the annihilation of two free quarks into the smallest allowed number of gluons. The states with $J=0,2$ are allowed to annihilate into two gluons. Including first-order QCD corrections the decay rates are given by [24]

$$\Gamma_{gg}(2P_2) = \frac{8}{5} \frac{\alpha_s^2}{m_b^4} |\Psi'(0)|^2 \left[1 + \frac{\alpha_s}{\pi} \right], \quad (7.1)$$

$$\Gamma_{gg}(2P_0) = \frac{6\alpha_s^2}{m_b^4} |\Psi'(0)|^2 \left[1 + 10.2 \frac{\alpha_s}{\pi} \right]. \quad (7.2)$$

To lowest order their ratio is $\frac{15}{4}$, independent of any parameters. For the state with $J=1$ the leading contribution to the annihilation width comes from annihilation into a quark pair and one gluon [25]:

$$\Gamma_{q\bar{q}g}(2P_1) = \frac{32}{9} \frac{\alpha_s^3}{m_b^4} |\Psi'(0)|^2 \ln(m_b \langle r \rangle), \quad (7.3)$$

where $\langle r \rangle$ is the mean radius of the $\chi_b(2P_1)$ state. If we assume that the gluons and quarks in the final states hadronize with unit probability the hadronic widths are identical to the annihilation widths. They have been evaluated, e.g., by Kwong and Rosner [8] using their values of the derivative of the wave function at zero quark separation $\Psi'(0)$ and $\alpha_s = 0.184 \pm 0.006$ obtained from the ratio $\Gamma_{\gamma gg}(\Upsilon) / \Gamma_{ggg}(\Upsilon)$ [26]. They find

$$\begin{aligned} \Gamma_{gg}(2P_2) &= (153 \pm 13) \text{ keV}, \\ \Gamma_{q\bar{q}g}(2P_1) &= (51 \pm 5) \text{ keV}, \\ \Gamma_{gg}(2P_0) &= (866 \pm 65) \text{ keV}. \end{aligned} \quad (7.4)$$

TABLE VIII. Electric dipole and hadronic widths of $\chi_b(2P)$ states.

Model	J	$\Gamma_{E1}(\chi_b(2P_J) \rightarrow \Upsilon(1S)\gamma)$ (keV)	$\Gamma_{E1}(\chi_b(2P_J) \rightarrow \Upsilon(2S)\gamma)$ (keV)	$\Gamma_{\text{had}}(2P_J)$ (keV)
KR	2	9.71	18.6	$89 \pm 11 \pm 11$
	1	9.25	15.8	$65 \pm 7 \pm 13$
	0	8.49	11.5	$343 \pm 118 \pm 58$
GRR	2	8.16	19.0	$82 \pm 10 \pm 11$
	1	7.77	16.1	$59 \pm 6 \pm 9$
	0	7.13	11.7	$313 \pm 108 \pm 42$
PF	2	10.0	18.7	$91 \pm 11 \pm 12$
	1	9.54	15.8	$66 \pm 7 \pm 14$
	0	8.76	11.6	$351 \pm 120 \pm 61$

The errors come from the uncertainty in α_s and the first-order QCD corrections.

These widths are too small to be measured directly. We can, however, derive them from the measurement of $B(\chi_b(2P_J) \rightarrow \Upsilon\gamma)$, given in Table VI. Let $\sum \Gamma_{E1}$ be the sum of the partial widths of all electric dipole decays of $\chi_b(2P_J)$. The hadronic width Γ_{had} of the $\chi_b(2P_J)$ state is then

$$\Gamma_{\text{had}} = \frac{\Gamma_{E1}(\chi_b(2P) \rightarrow \Upsilon\gamma)}{B(\chi_b(2P) \rightarrow \Upsilon\gamma)} - \sum \Gamma_{E1}. \quad (7.5)$$

The widths of the electric dipole transitions can be calculated by taking the dipole matrix element from potential model calculations. Values for $\Gamma_{E1}(\chi_b(2P_J) \rightarrow \Upsilon\gamma)$ are given in Table VIII, together with the values for the hadronic widths. We have used electric dipole matrix elements from three different potential models, the inverse scattering potential of KR [8], the semirelativistic model of GRR [12], and an updated Richardson potential [27] by Franzini (PF) [15].

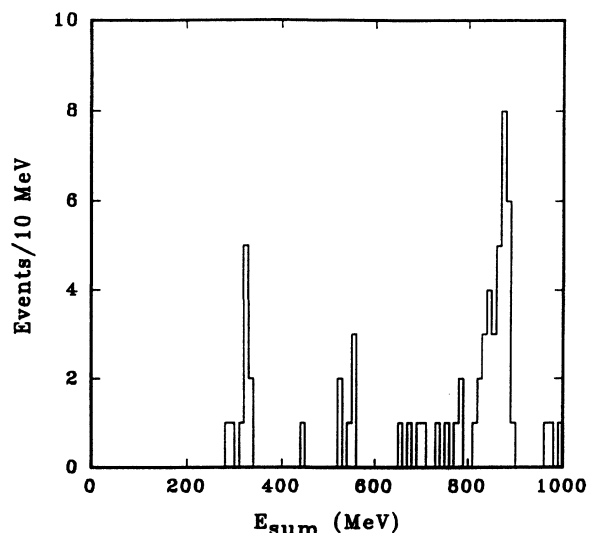
The variation between the values for the hadronic widths obtained using different models is small. The measured values of the hadronic widths are in qualitative agreement with the QCD predictions, although the two-gluon widths of the even spin states turn out to be somewhat smaller than expected. Their ratio agrees with the QCD expectation of $\frac{15}{4}$.

By solving the expressions for the annihilation rates of the $\chi_b(2P)$ states in Eqs. (7.1)–(7.3) for the strong coupling constant α_s , we can use the measured values of the hadronic widths to measure α_s . Using the value of $\Psi'(0)$ by Kwong and Rosner [8] we obtain $\alpha_s = 0.14 \pm 0.01, 0.20 \pm 0.02, 0.12 \pm 0.02$ for $J=2, 1, 0$. Using the value of $\Psi'(0)$ quoted by Franzini [15] we obtain correspondingly $0.16 \pm 0.01, 0.21 \pm 0.02$, and 0.14 ± 0.03 . These values are in agreement with the results of other methods of measuring α_s in the $b\bar{b}$ system [26].

VIII. THE REACTION $\Upsilon(3S) \rightarrow \Upsilon\pi^0\pi^0$

Apart from electromagnetic transitions, hadronic transitions between $b\bar{b}$ states are also possible. They proceed

via the emission of soft gluons which then convert into light hadrons. Of the possible hadronic transitions between $b\bar{b}$ states, only two-pion transitions between $\Upsilon(^3S_1)$ states have been observed. We have observed the transitions $\Upsilon(3S) \rightarrow \Upsilon\pi^0\pi^0$ in the exclusive mode, where the final Υ state is identified by its decay into an e^+e^- or a $\mu^+\mu^-$ pair. The selection criteria are similar to the ones for exclusive events described above, except that we now require four photons in the calorimeter. We only accept events, in which the four photons have at least 15 MeV energy each and are consistent with coming from the decay of two π^0 's, within the angular resolution of our detector. We refer to these events as $ll\pi\pi$ events. For the $\mu^+\mu^-$ channel our data are based on $1.18 \times 10^6 \Upsilon(3S)$ decays and we find 51 events, while for the e^+e^- channel we use $6.4 \times 10^5 \Upsilon(3S)$ decays and find 17 events [28]. Figure 11 shows the spectrum of the sum of the four photon energies. The two peaks at about 330 and 860 MeV indicate transitions between $\Upsilon(3S)$ or $\Upsilon(1S)$. The excess of events between 500 and 600 MeV is due to the process

FIG. 11. Sum of photon energies in $ll\pi\pi$ events.

$\Upsilon(3S) \rightarrow \Upsilon(2S) + X$, $\Upsilon(2S) \rightarrow \Upsilon(1S)\pi^0\pi^0$, where X is unobserved. In the events with electrons in the final state we confirm this by measuring the mass of the e^+e^- pair.

We determine the event detection efficiencies by analyzing a sample of Monte Carlo events in the same way as the data. We have studied the dependence of the efficiencies on the dipion mass and found that for the transition $\Upsilon(3S) \rightarrow \Upsilon(1S)\pi^0\pi^0$ the efficiency increases with dipion mass. For the transition $\Upsilon(3S) \rightarrow \Upsilon(2S)\pi^0\pi^0$ it does not depend on the dipion mass. Table IX lists the average values. If the pions are emitted with zero relative angular momentum, the angular distribution function of the leptons is $1 + \cos^2\vartheta_l$, where ϑ_l is the angle which the leptons form with the beams. However, higher even-relative angular momenta are allowed which would produce a flatter angular distribution. We generated the Monte Carlo sample with isotropic angular distribution for the leptons. A $1 + \cos^2\vartheta_l$ distribution would decrease the acceptance of the calorimeter by 17%. The values of ϵ given in Table IX are the average of these two extreme cases. A systematic error of 8.5% equal to the difference between this average value and the two individual values for the efficiencies has been added in quadrature with the error due to Monte Carlo statistics. The efficiencies for the transition $\Upsilon(3S) \rightarrow \Upsilon(2S)\pi^0\pi^0$ have also been corrected up by 7% to account for feed-down $\Upsilon(2S)$ events in which $\Upsilon(2S) \rightarrow \Upsilon(1S) + X$. This is the same fractional correction as for cascade events.

We find 10 events with $280 < E_{\text{sum}} < 350$ MeV, consistent with $\Upsilon(3S) \rightarrow \Upsilon(2S)\pi^0\pi^0$. Assuming lepton universality and using the efficiencies from Table IX we extract a branching ratio $B(\Upsilon(3S) \rightarrow \Upsilon(2S)\pi^0\pi^0) = (1.7 \pm 0.5 \pm 0.2)\%$. For the process $\Upsilon(3S) \rightarrow \Upsilon(1S)\pi^0\pi^0$ we find 33 events with $800 \text{ MeV} < E_{\text{sum}} < 900$ MeV. This gives $B(\Upsilon(3S) \rightarrow \Upsilon(1S)\pi^0\pi^0) = (2.2 \pm 0.4 \pm 0.3)\%$. Both results are consistent with isospin symmetry and the measured branching ratios into charged pions, $B(\Upsilon(3S) \rightarrow \Upsilon(2S)\pi^+\pi^-) = (2.5 \pm 0.5)\%$, $B(\Upsilon(3S) \rightarrow \Upsilon(1S)\pi^+\pi^-) = (3.7 \pm 0.3)\%$. These branching ratios have been obtained by combining the values from Refs. [6] and [29].

We perform a kinematic fit to all events with $E_{\text{sum}} > 700$ MeV, using seven constraints, four from energy-momentum conservation, two from the assumption that the photons are from π^0 decays and one from the invariant mass of the lepton pair, in order to obtain the invariant mass of the dipion system. Figure 12 shows the efficiency corrected invariant mass spectrum. The shape of the dipion mass distribution is consistent with that found in $\Upsilon(3S) \rightarrow \Upsilon(1S)\pi^+\pi^-$ events [29] but not

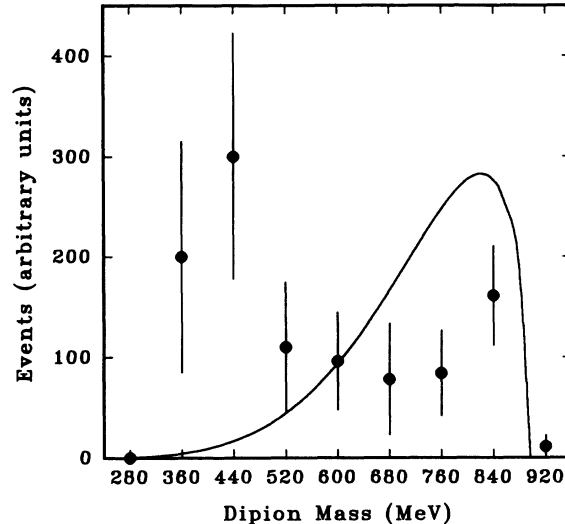


FIG. 12. Efficiency-corrected dipion mass spectrum from $\Upsilon(3S) \rightarrow \Upsilon(1S)\pi^0\pi^0$.

with the theoretical expectation [30] which is shown as a smooth curve superimposed on Fig. 12.

IX. CONCLUSIONS

By studying the electric dipole transitions from the $\Upsilon(3S)$ we have investigated the properties of the $\chi_b(2P)$ states. The measured rates of the transitions $\Upsilon(3S) \rightarrow \chi_b(2P)\gamma$ are in excellent agreement with potential model calculations, confirming the great success of these models in describing the spin-independent features of the $b\bar{b}$ system. By measuring the fine structure of the $\chi_b(2P)$ states we are able to probe the spin dependence of the interquark potential. While potential models agree qualitatively with our measurements in the dominance of the spin orbit over the tensor contribution, they do not reproduce the measured splittings well. Our measured value of the fine-structure ratio R for the $\chi_b(2P)$ states is smaller than R for the $\chi_b(1P)$ states, contrary to all potential model predictions. This disagreement could be explained by a mixing between the 2^3P_2 and 1^3F_2 states which would decrease R for the $\chi_b(2P)$ states.

Using the measured branching ratios for the electric dipole transitions from the $\chi_b(2P)$ states we have derived the hadronic widths of these states. The obtained values are consistent with lowest-order QCD calculations. We used the derived widths to measure the strong coupling constant α_s and found values in agreement with other determinations in the $b\bar{b}$ system.

The suppressed cascade transition $\Upsilon(3S) \rightarrow \chi_b(1P)\gamma \rightarrow \Upsilon(1S)\gamma\gamma$ has been seen for the first time. The branching ratios obtained from exclusive and inclusive channels are in good agreement. We have set upper limits on production of η_b and $\Upsilon(1D)$ states.

We have also presented a first measurement of the $\pi^0\pi^0$ transitions from the $\Upsilon(3S)$. Branching ratios and the dipion invariant mass spectrum from the transition $\Upsilon(3S) \rightarrow \Upsilon(1S)\pi^0\pi^0$ are in good agreement with observations of the charged pion transitions and isospin conser-

TABLE IX. Efficiencies for $\Upsilon(3S) \rightarrow \Upsilon\pi^0\pi^0$.

Transition	ϵ (%)
$\Upsilon(3S) \rightarrow uu(1S)\pi^0\pi^0, \Upsilon(1S) \rightarrow \mu\mu$	3.6 ± 0.4
$\Upsilon(1S) \rightarrow ee$	2.5 ± 0.3
$\Upsilon(3S) \rightarrow \Upsilon(2S)\pi^0\pi^0, \Upsilon(2S) \rightarrow \mu\mu$	2.5 ± 0.4
$\Upsilon(2S) \rightarrow ee$	2.1 ± 0.3

vation. The invariant mass spectrum does not agree with theoretical expectations.

ACKNOWLEDGMENTS

We would like to thank the CESR staff for their efforts in providing us with excellent running conditions. We

acknowledge the contributions of S. B. Sontz and T. K. Kaarsberg during the early stages of the experiment. Thanks go to Dave Winter for his work on the electronics for the second half of the data taking period. We also wish to thank Jonathan Rosner and Paula Franzini for helpful discussions. This work was supported in part by the National Science Foundation.

-
- [1] M. Narain *et al.*, Phys. Rev. Lett. **66**, 3113 (1991).
 - [2] U. Heintz *et al.*, Phys. Rev. Lett. **66**, 1563 (1991).
 - [3] J. Lee-Franzini, Nucl. Instrum. Methods **A263**, 35 (1988); P. M. Tuts, *ibid.* **A265**, 243 (1988); R. D. Schamberger *et al.*, *ibid.* **A309**, 450 (1991).
 - [4] R. Engelmann *et al.*, Nucl. Instrum. Methods **216**, 45 (1983).
 - [5] CUSB Collaboration, D. Peterson *et al.*, Phys. Lett. **114B**, 277 (1982).
 - [6] Particle Data Group, J. J. Hernández *et al.*, Phys. Lett. B **239**, 1 (1990).
 - [7] For $J=0$ there is only an upper limit to the branching ratio which was used in the fit.
 - [8] W. Kwong and J. L. Rosner, Phys. Rev. D **38**, 279 (1988).
 - [9] CLEO Collaboration, R. Morrison *et al.*, Phys. Rev. Lett. **67**, 1696 (1991).
 - [10] R. Ford and W. Nelson, Report No. SLAC-210, 1978 (unpublished).
 - [11] L. S. Brown and R. N. Cahn, Phys. Rev. D **13**, 1195 (1976).
 - [12] S. Gupta, S. F. Radford, and W. W. Repko, Phys. Rev. D **34**, 201 (1986).
 - [13] P. Moxhay and J. L. Rosner, Phys. Rev. D **28**, 1132 (1983).
 - [14] R. McClary and N. Byers, Phys. Rev. D **28**, 1692 (1983).
 - [15] P. J. Franzini, LBL Report No. 30440, 1991 (unpublished).
 - [16] L. P. Fulcher, Phys. Rev. D **39**, 295 (1989).
 - [17] J. Pantaleone, S.-H. H. Tye, and Y. J. Ng, Phys. Rev. D **33**, 777 (1986).
 - [18] Y. P. Kuang and T. M. Yan, Phys. Rev. D **24**, 2874 (1981); M. B. Voloshin, Yad. Fiz. **43**, 1571 (1986) [Sov. J. Nucl. Phys. **43**, 1011 (1986)].
 - [19] Scaled from $B_{\mu\mu}(1S)$ using the CUSB measurement of $\Gamma_{ggg}(\Upsilon(1S))/\Gamma_{\mu\mu}(\Upsilon(1S))$, T. Kaarsberg *et al.*, Phys. Rev. Lett. **62**, 2077 (1989).
 - [20] Figure 3 in Ref. [2].
 - [21] E. Eichten *et al.*, Phys. Rev. D **17**, 3090 (1979); **21**, 203 (1980).
 - [22] M. Campostrini, K. Moriaty, and C. Rebbi, Phys. Rev. Lett. **57**, 44 (1986).
 - [23] J. L. Rosner, in *Experimental Meson Spectroscopy—1983*, Proceedings of the 7th International Conference, Upton, New York, 1983, edited by S. J. Lindenbaum, AIP Conf. Proc. No. 113 (AIP, New York 1984), p. 461.
 - [24] R. Barbieri, R. Gatto, and R. Kögerler, Phys. Lett. **60B**, 183 (1976); R. Barbieri, M. Caffo, R. Gatto, and M. Remiddi, Nucl. Phys. **B192**, 61 (1981).
 - [25] R. Barbieri and R. Gatto, Phys. Lett. **61B**, 465 (1976).
 - [26] W. Kwong, P. B. Mackenzie, R. Rosenfeld, and J. L. Rosner, Phys. Rev. D **37**, 3210 (1988).
 - [27] J. L. Richardson *et al.*, Phys. Lett. **82B**, 272 (1979).
 - [28] The event sample for the e^+e^- channel is smaller because the earlier half of the data was not reanalyzed for this transition.
 - [29] CLEO Collaboration, I. C. Brock *et al.*, Phys. Rev. D **43**, 1448 (1991).
 - [30] T. M. Yan, Phys. Rev. D **22**, 1652 (1980).